Journal of Machine Engineering, 2026, Vol. 26
ISSN 1895-7595 (Print) ISSN 2391-8071 (Online)

Received*: 11 September 2025* / Accepted: *08 January 2026* / Published online: *25 February 2026*

FEM thermal simulation,
laser keyhole welding,
overlap welding of thin plates,
optimum processing conditions

Ikuo TANABE[1*]

DEVELOPMENT OF FEM THERMAL SIMULATION TECHNIQUE FOR LASER KEYHOLE WELDING

In laser keyhole welding, large energy is irradiated over a small area, making it extremely difficult to find the optimum processing conditions to achieve the desired welding specifications. In particular, the search for optimum processing conditions is difficult in the overlap welding of thin plates, and a great deal of time and effort is required to find the best conditions. Therefore, in this research, a new FEM (Finite Element Method) thermal simulation technique for laser keyhole welding was developed and evaluated. The FEM thermal simulation utilized SolidWorks software with implicit solution. The FEM simulation defines the simulated thermal conductivities with temperature- dependent for the molten (fluid) and evaporated (gas) portions, respectively, allowing solid elements to simulate workpiece melting and evaporation. The travelling irradiation of the laser beam was simulated by the time dependence of the heat source. The proposed technique was evaluated in some experiments with several conditions. As a result, it had been concluded that the proposed technique could calculate with high accuracy for the desired welding specifications, and the proposed technique was very effective for the search of the optimum processing conditions.

1. INTRODUCTION

Laser processing is widely used in various fields such as automotive, aerospace, and electronics industries [1–3]. Laser welding irradiates a large amount of energy onto a small area, making it extremely difficult to find the optimal processing conditions to achieve the desired welding specifications [4–17]. In particular, it is difficult to find the optimum processing conditions for overlap welding of thin plates, and the search for the optimum processing conditions requires a great deal of time and labour. On the other hand, there has been a recent demand for technology for overlap welding of thin aluminium and stainless-steel plates for battery housings of electric vehicles [18]. FSW (Friction Stir Welding) can be used to reliably weld these thin plates together, but the long processing time makes it

[1] Technical and Management Engineering, Sanjo City University, Japan
[*] E-mail: : tanabe.ikuo@sanjo-u.ac.jp
https://doi.org/10.36897/jme/216501

extremely difficult to be productive [19]. In addition, the product size is large due to the large area of the joining area [20].

In this paper, a new FEM thermal simulation technique for laser keyhole welding was developed and evaluated. The FEM transient thermal simulation using the commercial software SolidWorks 2023 with implicit solution was used for the technique. The simulated thermal conductivities with temperature- dependent for the molten (fluid) and evaporated (gas, keyhole) regions of the workpiece was used for the technique, respectively. And both melting and evaporation phenomena in the workpiece were simulated using the solid elements. No element removal or remeshing was required during this calculation, so the calculations can be performed directly in SolidWorks 2023. In addition, the traveling irradiation of the laser beam was simulated by the time dependence of the heat source. The technique was experimented and evaluated on an overlap welding of stainless steel SUS304. SUS304 stainless steel was used as the workpiece for analysis, experimentation, and consideration. Furthermore, as laser keyhole welding involves both melting and evaporation, the FEM transient thermal simulation with implicit solution were currently difficult to perform, and no relevant references has been found.

2. DESCRIPTION OF LASER KEYHOLE WELDING

Laser welding is a welding process in which a laser beam is irradiated to a workpiece locally for a short time [6, 7]. It is necessary to supply a sufficient amount of energy for melting, but control on the millisecond order is required to prevent insufficient melting or, conversely, fusion breakdown. A keyhole is a cavity generated by evaporation on the workpiece surface directly under the torch, which enables deep penetration welding [9]. This welding process is also prone to spatter (dispersal of molten metal during welding). The welding of SUS304 [21] is also a keyhole weld.

A schematic view of keyhole welding by laser traveling irradiation was shown in Fig. 1(a), and a photograph of keyhole welding. keyholes generated by the evaporation of SUS304 move as the laser travels was shown in Fig. 1(b). There was a molten area of SUS304 around the keyhole, and the molten area also moves along with the movement of the keyhole.

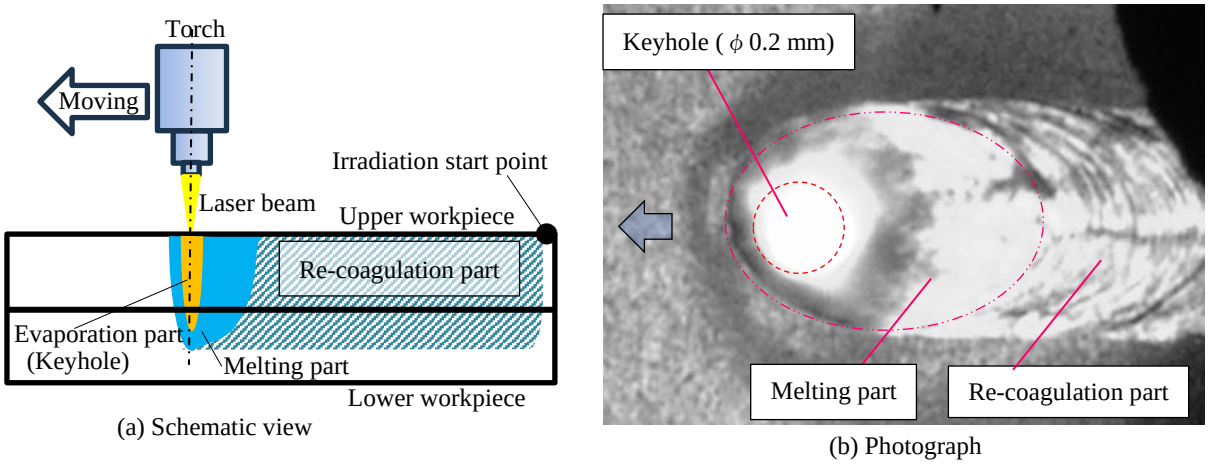

(a) Schematic view

(b) Photograph

Fig. 1 Schematic view and photograph of the laser keyhole welding

This molten area was wider on the opposite side of the travel direction due to the laser travel irradiation, and was used to bury the keyhole after the torch travels.

3. ALGORITHM FOR FEM THERMAL SIMULATION TECHNIQUE OF LASER KEYHOLE WELDING

An inexpensive, quick, and easy technique to find optimal processing conditions using the commercial FEM software SolidWorks 2023 was developed. Specifically, a FEM thermal simulation technique to analyse the melting and evaporation phenomena of the workpiece was firstly developed. Next, a FEM thermal simulation technology for laser travel irradiation was developed. Finally, a technique to simulate the heat input of laser irradiation by a ring torch, which was often used to prevent spatter was also developed.

3. 1. LASER KEYHOLE WELDING USED IN THIS RESARCH AND ITS FEM MODEL

As shown in Fig. 2, the maximum top width $T_{w\text{-}max}$, maximum penetration depth d_{max}, and maximum penetration width $M_{w\text{-}max}$ of the joining surface were often used as the required welding specifications for superimposed laser welding of 2 workpieces with SUS304. These three specifications were also for the evaluation of the proposed technique. As shown in Fig. 3, laser welding was performed with the Ring-type torch on two 150 mm × 100 mm × 3 mm stainless steel plates in an overlap welding process. The fibre laser processing machine (AMADA, BREVIS-1212AJ, Pulse peak power 3000W, laser source- fibre laser with laser diode excitation) was used for that welding. Argon gas was used as the assist gas. The processing conditions and experimental results (penetration specifications) were shown in Table 1, and the photographs after the laser welding process were shown in Fig. 4 to 8. The experimental result for Test No.1 in Fig. 4 was used to calculate the simulated thermal conductivities with temperature- dependent in Section 3.2. The other experimental results were used to evaluate the proposed technique.

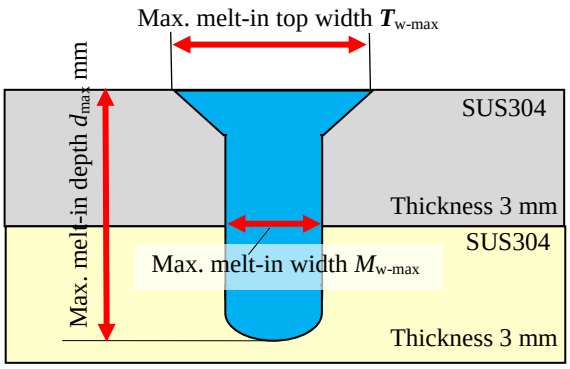

Fig. 2. Definition of quality evaluation factors for laser keyhole welding

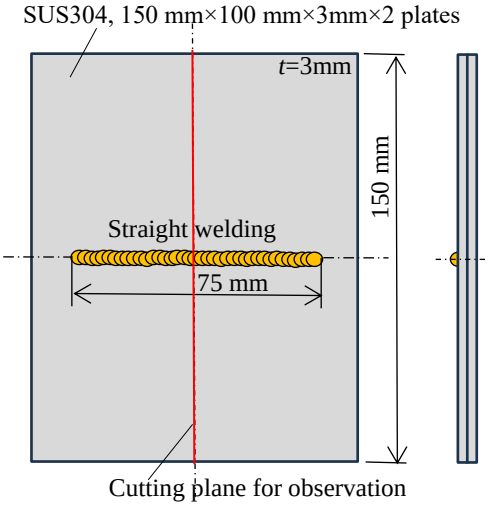

Fig. 3. Schematic view of the evaluation experiment

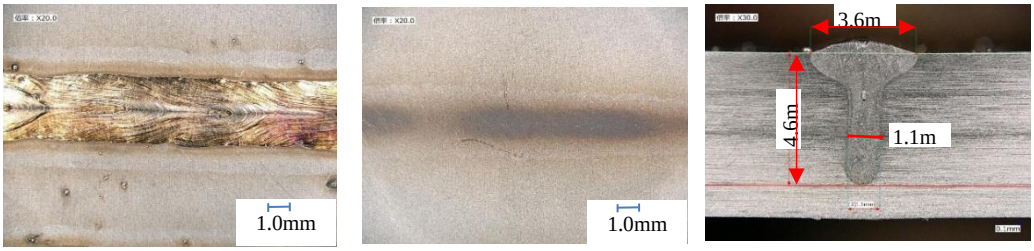

(a) Surface (b) Back (c) Cross-section

Fig. 4. Photograph after laser welding__Test No. 1

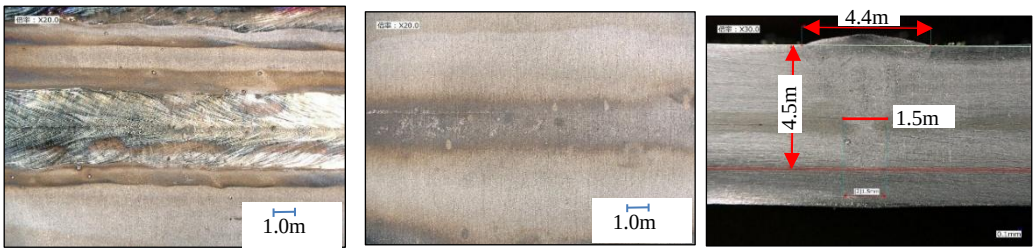

(a) Surface (b) Back (c) Cross-section

Fig. 5. Photograph after laser welding__Test No. 2

(a) Surface (b) Back (c) Cross-section

Fig. 6. Photograph after laser welding__Test No. 3

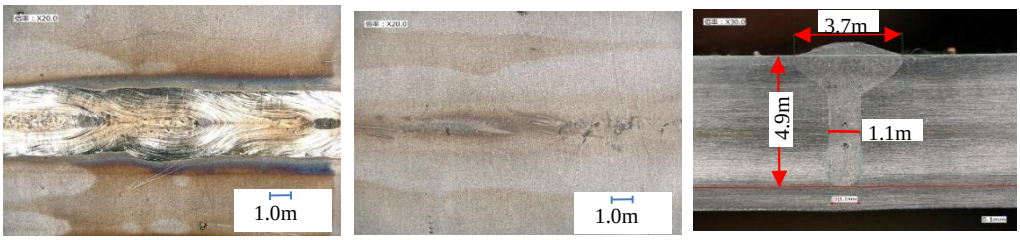

(a) Surface (b) Back (c) Cross-section

Fig. 7. Photograph after laser welding__Test No. 4

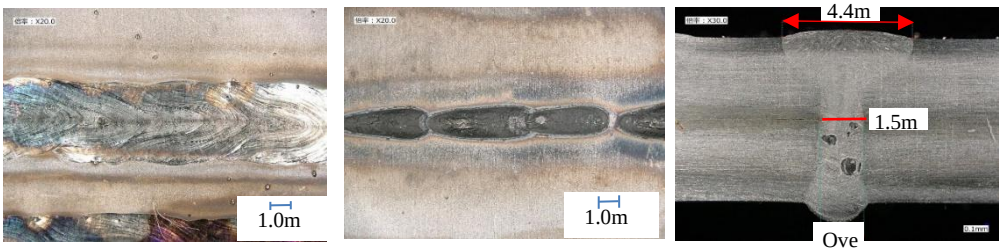

(a) Surface (b) Back (c) Cross-section

Fig. 8. Photograph after laser welding__Test No. 5

The FEM model for the analysis of overlap welding with stainless-steel by FEM thermal simulation was shown below. As shown in Figure 9, in the superposition welding of two stainless steel sheets with10.8 mm×10.8 mm×3 mm (SUS304, solid-state thermal conductivity 16.3 W/mK, melting point 1450 °C, boiling point 2862 °C), a ring-type torch (torch ring outer diameter ϕ 0.54 mm) was used for the FEM thermal simulations were performed for laser irradiation with centre irradiation energy E_{in} = 1.0 kW, ring irradiation energy E_{out} = 2.0 W, and feed rate F = 16.7 mm/s. This was the data of No. 1 in Table 1. The FEM model was a 1/2 model of the original model. The FEM model (10.8 mm×10.8 mm×3 mm×2 sheets) was approximately 1/10th the length and width dimensions of the experimental specimens (150 mm×100 mm×3 mm×2 sheets), but the validity of this FEM model size was clear from the preliminary analysis (no temperature changes on the point A_E the analysis). The heat transfer coefficient was set to 0 W/mK for the adiabatic surfaces and 12 W/mK for the other surfaces.

Table 1. Processing conditions and experimental results of laser welding of SUS304 (melting specifications). The irradiation distance was the distance between the workpiece and the torch

Test No.	Laser processing conditions					Experimental results（melting specifications）		
	Center Power kW	Ring Power kW	Irradiation travel speed m/min	Gas flow rate ℓ/min	Irradiation distance mm	Top width T_w mm	Mid width M_w mm	Melt-in depth d mm
1	1.0	2.0	1.0	30	366	3.6	1.1	4.6
2	0.5	1.7	0.5	30	370	4.4	1.5	4.5
3	0.9	1.9	1.0	30	370	3.5	1.0	4.4
4	1.1	2.1	1.0	30	370	3.7	1.1	4.9
5	0.7	1.9	0.5	30	368	4.4	1.5	6.0 over

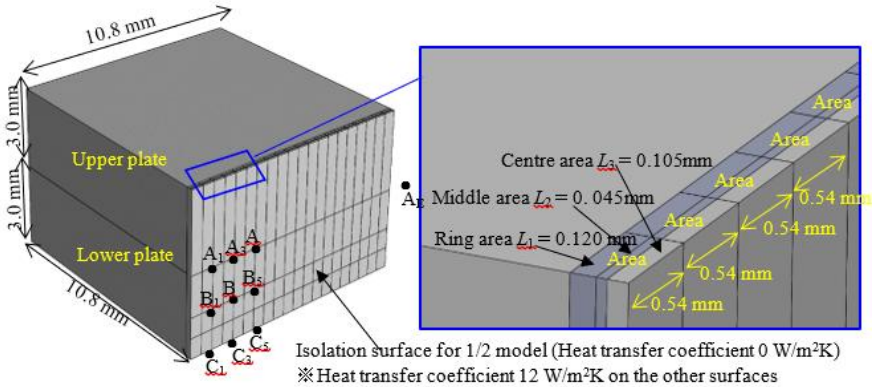

Fig. 9. FEM model for laser keyhole welding of SUS 304（1/2 model)

3. 2. FEM THERMAL SIMULATION MODEL FOR MELTING AND EVAPORATION PHENOMENA

In order to perform FEM thermal simulation of laser keyhole welding, melting and evaporation phenomena were simulated by setting the simulated thermal conductivities with temperature-dependent in the workpiece while maintaining the equivalent heat capacity (irradiation energy = incremental heat capacity in the workpiece).

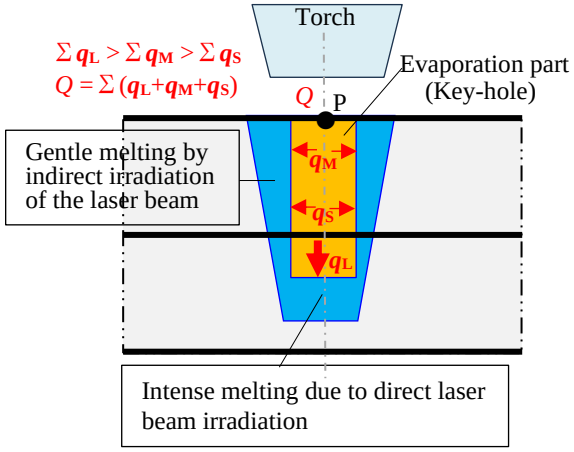

(a) Schematic view of heat inflow from the keyhole to the melt region and the flow state in the melt region at that time

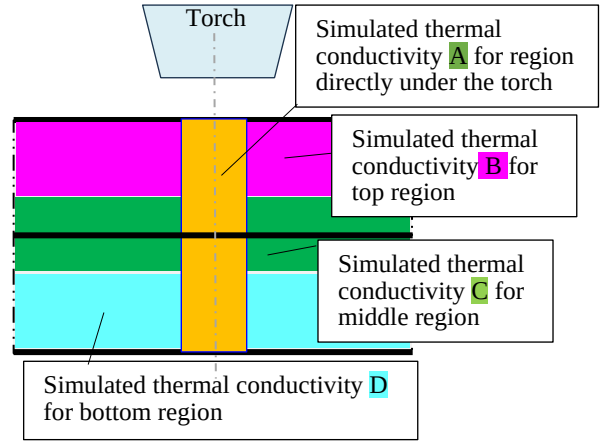

(b) Setting up four thermal conductivity regions taking into account the heat inflow from the keyhole to the melt region

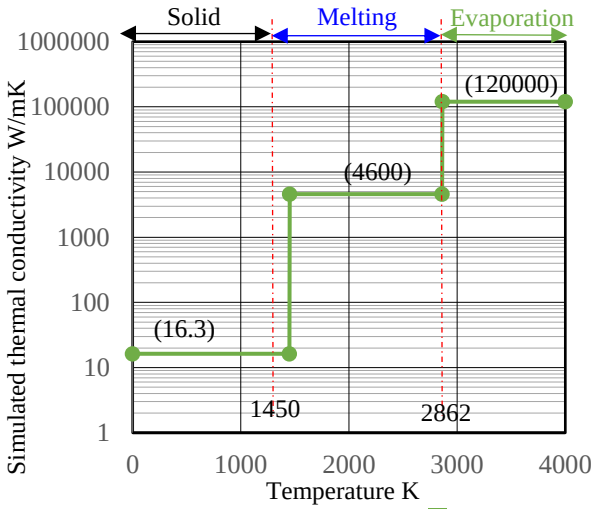

(c) Simulated thermal conductivity A for region directly under the torch

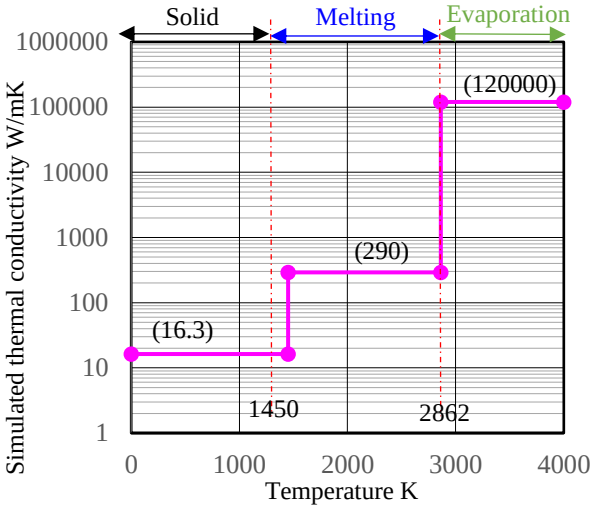

(d) Simulated thermal conductivity B for top region

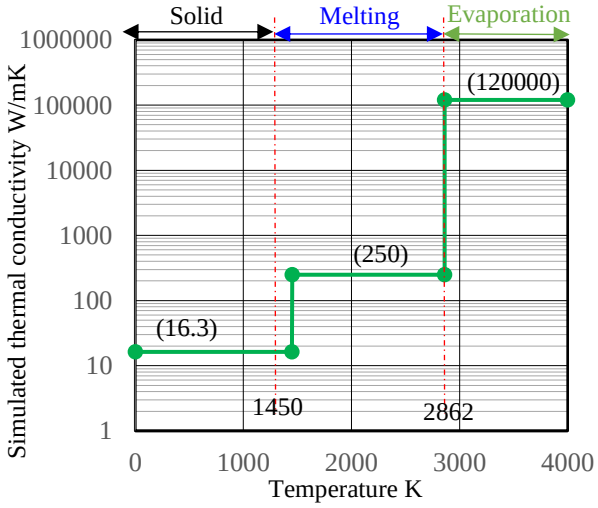

(e)Simulated thermal conductivity C for middle region

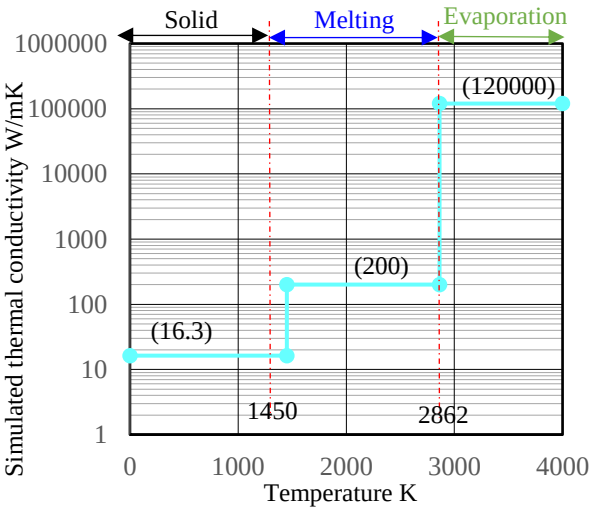

(f)Simulated thermal conductivity D for bottom region

Fig. 10. Four simulated thermal conductivity curves for new FEM simulation

The analysis of melting (fluid) and evaporation (gas) phenomena was difficult with current FEM thermal simulations. Therefore, the simulated thermal conductivities with temperature- dependent were used for the FEM thermal simulation. Since it was difficult to delete or remeshing these elements during the analysis in SolidWorks 2023, the only solid elements were used for the analysis.

Four simulated thermal conductivity curves for FEM thermal simulations were shown in Figure 10. As shown in Fig. 10(a), the incident light was diffusely reflected at the boundary between the keyhole and the molten area, and all of the laser irradiation energy Q W was absorbed into the molten area. This phenomenon could be simulated by increasing the thermal conductivity so that the temperature of the keyhole area (orange) did not exceed the boiling point. The thermal conductivity of the workpiece was made extremely large (120000 W/mK) when above the boiling point, so that the temperature T_A at point P in Fig. 10(a) was the boiling point. By defining this temperature dependent thermal conductivity in the FEM model, the element that has reached the boiling point becomes an element that only conducts the input irradiation energy Q W directly to the molten region, although it still existed as an element. Most of the irradiation energy was applied to the bottom of the keyhole, so that a large amount of energy ($\Sigma\, q_L$ W) was supplied below the bottom of the keyhole. The boiling was accelerated, and the keyhole depth was increased. Furthermore, the molten region below the keyhole bottom was in a state of intense convection accompanied by boiling, and the depth of the molten region was also deepened by the increase in its thermal conductivity. Next, the diffusely reflected laser beam inside the keyhole was irradiated and absorbed by the sides of the keyhole, and $\Sigma\, q_M$ W and $\Sigma\, q_S$ W of energy was supplied to the molten area on the sides of the keyhole. However, the amount of energy supplied to the sides of the keyhole was not as much as that of the bottom of the keyhole ($\Sigma q_L > \Sigma q_M > \Sigma q_S$) and was not enough to significantly expand the molten area on the sides of the keyhole. In order to simulate these elements in a FEM thermal simulation, it was necessary to define anisotropic thermal conductivity for the elements directly under the torch and the other elements, but SolidWorks 2023 does not have that capability. Therefore, as shown in Figure 10(b), it was decided to define the simulated thermal conductivities with temperature- dependent for four regions: the one region directly under the torch and the other three regions (the top, middle and bottom regions). Four temperature-dependent simulated thermal conductivity curves were explored. Four curves were determined using the sequential substitution method to precisely calculate the welding specifications ($T_{w\text{-}max}$, d_{max} and $M_{w\text{-}max}$) for Test No. 1 in Table 1 and Fig. 4. Four curves of Fig. 10 (c), (d), (e), (f) were the simulated thermal conductivity A for region directly under the torch, B for top region, C for middle region and D for bottom region respectively. These four curves provide the database for calculating welding specifications for overlap welding of stainless-steel SUS 304. Therefore, FEM simulations of the welding specifications of Test No. 2, No. 3, No. 4 and No. 5 were also used the same database.

3. 3. FEM THERMAL SIMULATION FOR LASER BEAM TRAVELING IRRADIATION

FEM thermal simulation for Test No.1 in Figure 11 and Table 2 was used for the explanation. Here, the example of FEM thermal simulation was shown for the condition with

torch diameter $D = \phi$ 0.54 mm, irradiation energy E =3000 W, and feed rate F =1 m/min= 16.7 mm/s. The model was 1/2 of the original model (to reduce calculation time and to make it easier to observe the weld), so the irradiation energy was 1500 W, 1/2 of E=3000 W. The 1/2 split surface was an adiabatic surface, and the heat transfer coefficient = 0 W/m^{2}K was set. Each laser irradiation area of 0.27 mm × 0.54 mm (0.27 mm = half of the torch diameter, 0.54 mm = torch diameter) was set to simulate a half circle of the torch in a rectangle. As shown in Table 2, energy (1500 W × 0.0323 s) was input to each region for Δt = 0.0323 s (= long dimension of the region D mm/feed rate F mm/s), and FEM transient thermal simulations were performed continuously in coupled analysis.

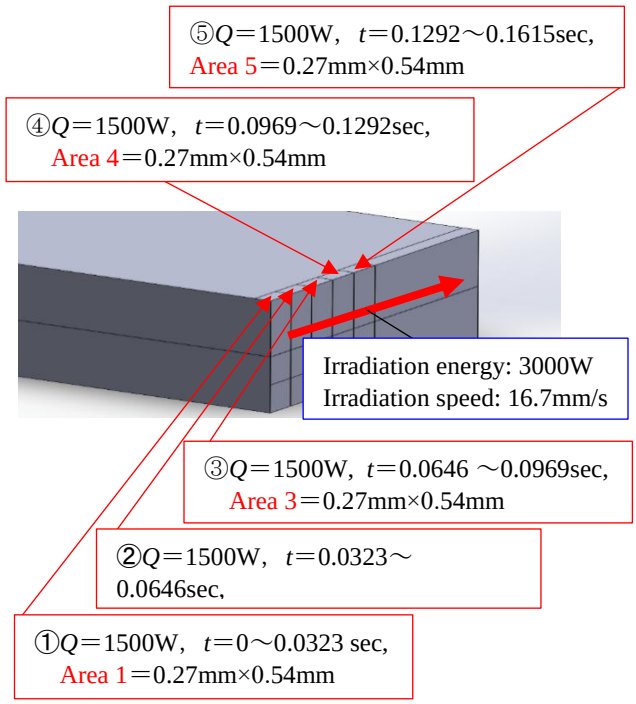

Fig. 11. Relationship between the irradiation energy and each area for the travelling irradiation

Table 2 Irradiation energy table on each area at FEM thermal simulation for SUS304 laser keyhole welding

Time t sec	0～0.0323	0.0323～0.0646	0.0646～0.0969	0.0969～0.1292	0.1292～0.1615
Area 1	Q_1 Q_2 Q_3	—	—	—	—
Area 2	—	Q_1 Q_2 Q_3	—	—	—
Area 3	—	—	Q_1 Q_2 Q_3	—	—
Area 4	—	—	—	Q_1 Q_2 Q_3	—
Area 5	—	—	—	—	Q_1 Q_2 Q_3

※In case of Test No.1: Q=1500 W, Q_1 (heat supplied to ring area)=479 W, Q_2 (heat supplied to middle area)=186 W and Q_3 (Heat supplied to centre area)=835 W calculated by irradiation energy of centre E_{in} = 1.0 kW, irradiation energy of ring E_{out} = 2.0 kW, eq. (1), (2), (3).

The initial temperature of the workpiece in the FEM transient thermal simulation in Area 1 was set to 0 K. The initial temperature of the workpiece in the FEM transient thermal simulation in Area 2 and beyond was set to the final analysis results of the previous Area to ensure continuous analysis. This enabled the simulation of continuous laser irradiation at a feed rate of F = 16.7 mm/s (≈ 0.54 mm / 0.0323 sec).

3. 4. FEM THERMAL SIMULATION FOR BEAM IRRADIATION WITH RING-TYPE TORCH

Spatter generation during welding was a major problem in laser welding, and ring-type torches were often used to prevent spatter generation. The ring torch shown in Fig. 12 was used for welding. As shown in Fig. 13, when setting the laser irradiation energy, the heat input region was set in three layers (D×L_1, D×L_2, and D×L_3), and the irradiation energies Q_1, Q_2,

and Q_3 W were input for each according to the scanning speed. As shown in Figure 14, three layers of heat input areas (red lines) were aligned on the half of a ring torch with a centre diameter of ϕd mm, a ring inner diameter of ϕD_r mm, and a ring outer diameter (= laser bore diameter) of ϕD mm, and the supply energies Q_1, Q_2, and Q 3 W were calculated from the irradiation area and irradiation energy of each heat input region by their area ratios.

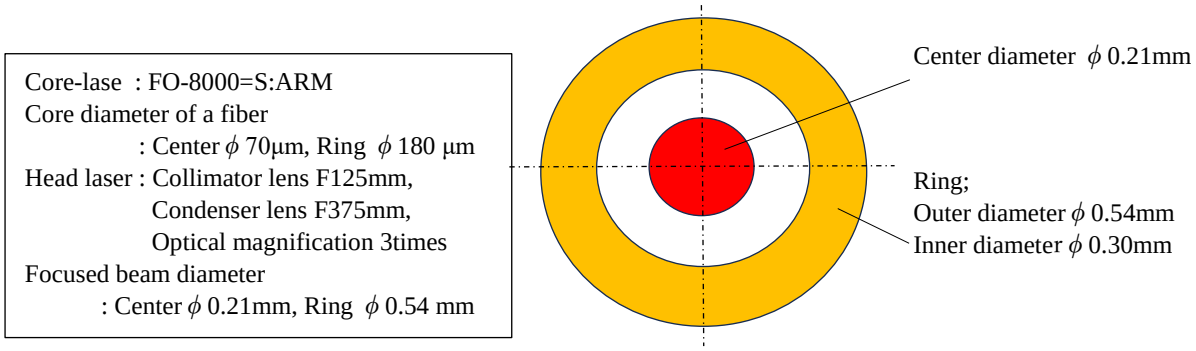

Fig. 12. Specification of the ring type laser torch

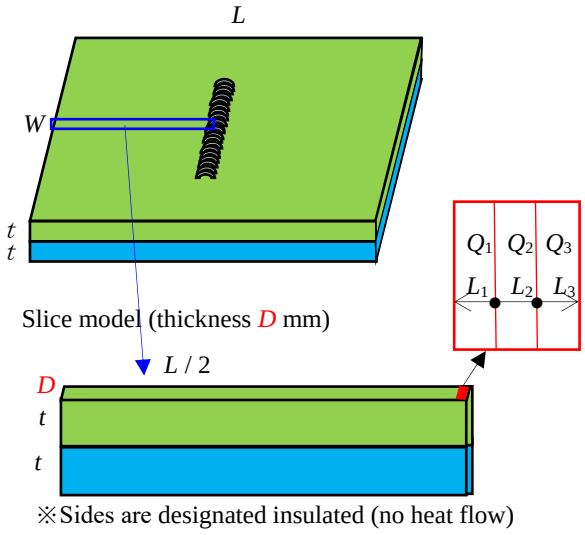

Fig. 13. Heat generation setting for analysis with ring torch

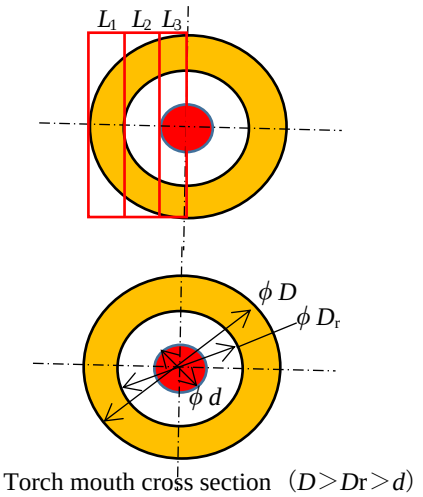

Fig. 14. Specification of the ring torch

Specifically, the long dimension D mm of each heat input area was equal to the ring outer diameter ϕD mm, and the width (short side) of each heat input area was $L_1 = D/2\text{-}D_r/2$ mm, $L_2 = D_r/2\text{-}d/2$ mm, $L_3 = d/2$ mm. Assuming that the centre irradiation energy was E_{in} W and the ring irradiation energy was E_{out} W, the supply energies Q_1, Q_2, and Q_3 W of each heat input region could be calculated from the irradiation area ratio of each heat input region using Equations (1), (2), and (3).

$$Q_1 = E_{out}\,[D^2(\,\mathrm{Cos}^{-1}(D_r / D) - \mathrm{Cos}(\mathrm{Cos}^{-1}(D_r / D))\mathrm{Sin}(\mathrm{Cos}^{-1}(D_r / D)))\,/4]\,/ \\ 3.14(D^2/4 - D_r{}^2/4) \tag{1}$$

$$Q_2 = E_{out}[D^2(\,\mathrm{Cos}^{-1}(d / D)\, - \mathrm{Cos}\,(\mathrm{Cos}^{-1}(d / D))\mathrm{Sin}\,(\mathrm{Cos}^{-1}(d / D)))\,/4 - \mathrm{Dr}^2(\,\mathrm{Cos}^{-1}(\mathrm{d} / D_r) \\ - \mathrm{Cos}\,(\mathrm{Cos}^{-1}(\mathrm{d} / D_r))\mathrm{Sin}\,(\mathrm{Cos}^{-1}(\mathrm{d} / \mathrm{Dr})))\,/4\, - D^2(\,\mathrm{Cos}^{-1}(D_r / D) - \mathrm{Cos}(\mathrm{Cos}^{-1}(D_r /$$

$$D))\mathrm{Sin}(\mathrm{Cos}^{-1}(D_r / D))) /4] / 3.14(D^2/4 - D_r{}^2/4) \quad (2)$$

$$Q_3 = E_{out}[3.14(\mathrm{D}^2 - \mathrm{Dr}^2)/8 - D^2(\mathrm{Cos}^{-1}(d / D) - \mathrm{Cos}(\mathrm{Cos}^{-1}(d / D))\mathrm{Sin}(\mathrm{Cos}^{-1}(d / D))) /4 - \mathrm{Dr}^2(\mathrm{Cos}^{-1}(\mathrm{d} / \mathrm{Dr}) - \mathrm{Cos}(\mathrm{Cos}^{-1}(\mathrm{d} / \mathrm{Dr}))\mathrm{Sin}(\mathrm{Cos}^{-1}(\mathrm{d} / \mathrm{Dr}))) /4 - 2D^2(\mathrm{Cos}^{-1}(D_r / D) - \mathrm{Cos}(\mathrm{Cos}^{-1}(D_r / D))\mathrm{Sin}(\mathrm{Cos}^{-1}(D_r / D))) /4] / 3.14(D^2/4 - D_r{}^2/4) + E_{in}/2 \quad (3)$$

Each area in Figure 6 was divided into three planes in advance at the CAD stage, and the heat input areas ($D\times L_1$, $D\times L_2$, and $D\times L_3$) were input with the heat quantities Q_1, Q_2, and Q_3 W calculated by Equations (1), (2), and (3), and the continuous FEM unsteady thermal simulation described was repeated. As shown in Table 3, the analysis conditions for FEM unsteady thermal simulation with1/2 model were calculated.

Table 3. Analysis conditions for FEM unsteady thermal simulation (Irradiation energy was 1/2 model value)

Test No.	Laser processing conditions			Irradiation arear			Irradiation time	Irradiation energy		
	Center Power kW	Ring Power kW	Irradiation travel speed m/min	Center area $D\times L_1$ mm	Middle area $D\times L_2$ mm	Ring area $D\times L_3$ mm	Irradiation time in each area sec	$Q_1$for Ring W	Q_2 for Middle W	Q_3 for Centre W
1	1.0	2.0	1.0	0.54× 0.105	0.54× 0.045	0.54× 0.120	0.0323	479	186	835
2	0.5	1.7	0.5	0.54× 0.105	0.54× 0.045	0.54× 0.120	0.0646	407	158	535
3	0.9	1.9	1.0	0.54× 0.105	0.54× 0.045	0.54× 0.120	0.0323	455	177	768
4	1.1	2.1	1.0	0.54× 0.105	0.54× 0.045	0.54× 0.120	0.0323	503	195	902
5	0.7	1.9	0.5	0.54× 0.105	0.54× 0.045	0.54× 0.120	0.0646	455	177	668

4. EVALUATION OF THE PROPOSED FEM THERMAL SIMULATION TECHNIQUE

The results of the analysis using the proposed FEM thermal simulation were shown in Figures 15 to 19. Temperature distributions and welding specifications were shown. In each figure, the blue line was the melting boundary.

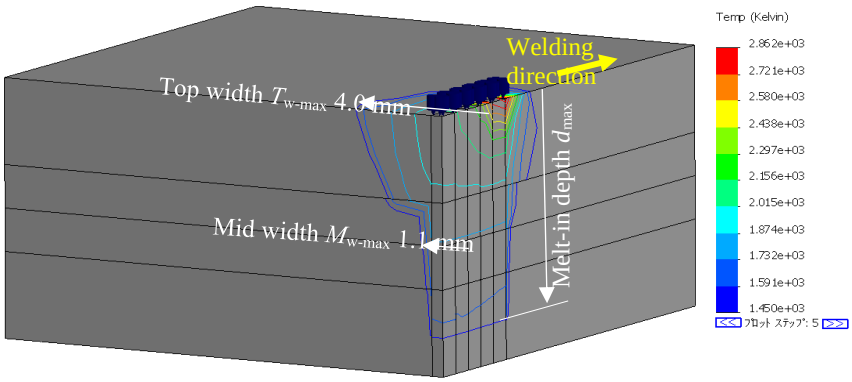

Fig. 15. Temperature distribution at t=0.1615 sec regarding Test No. 1 (Blue line: melting point)

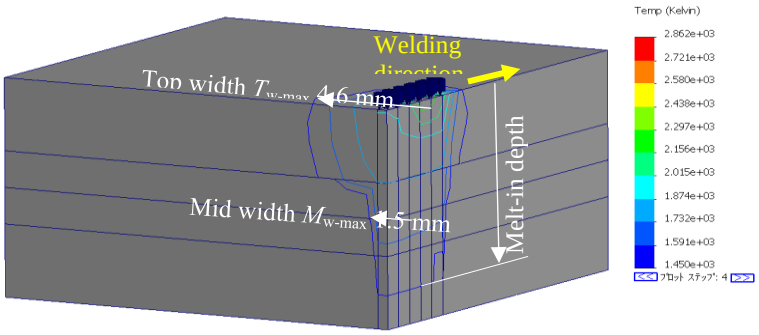

Fig. 16. Temperature distribution at t=0.323 sec regarding Test No. 2 (Blue line: melting point)

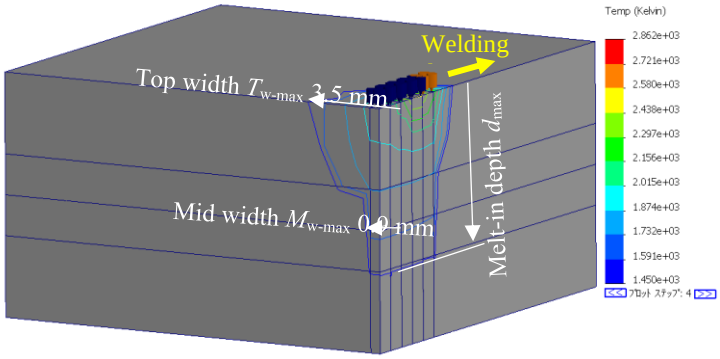

Fig. 17 Temperature distribution at t=0.1615 sec regarding Test No. 3 (Blue line: melting point)

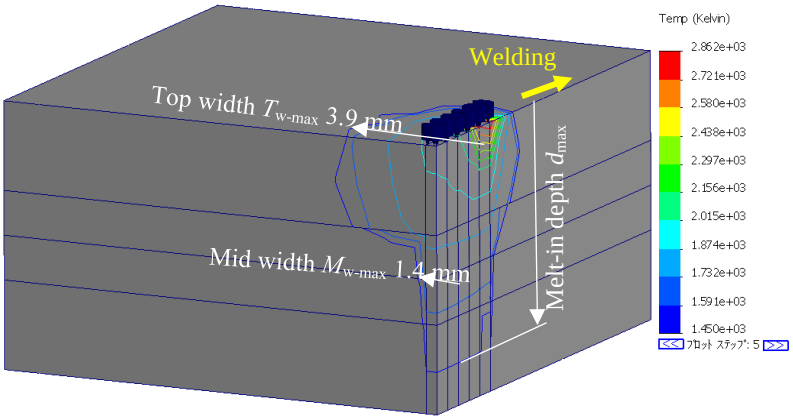

Fig. 18. Temperature distribution at t=0.1615 sec regarding Test No. 4 (Blue line: melting point)

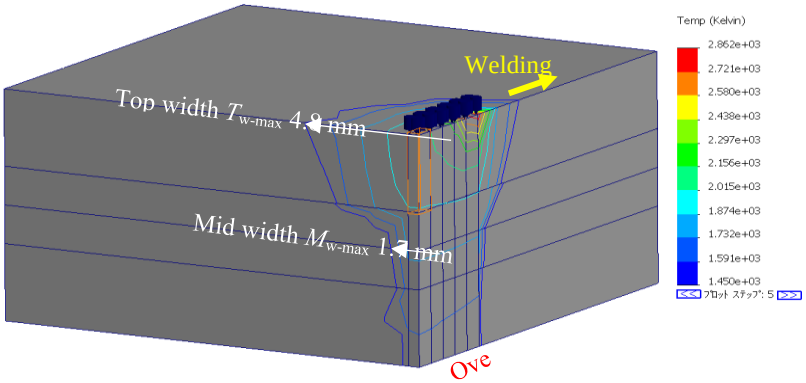

Fig. 19. Temperature distribution at t=0.323 sec regarding Test No. 5

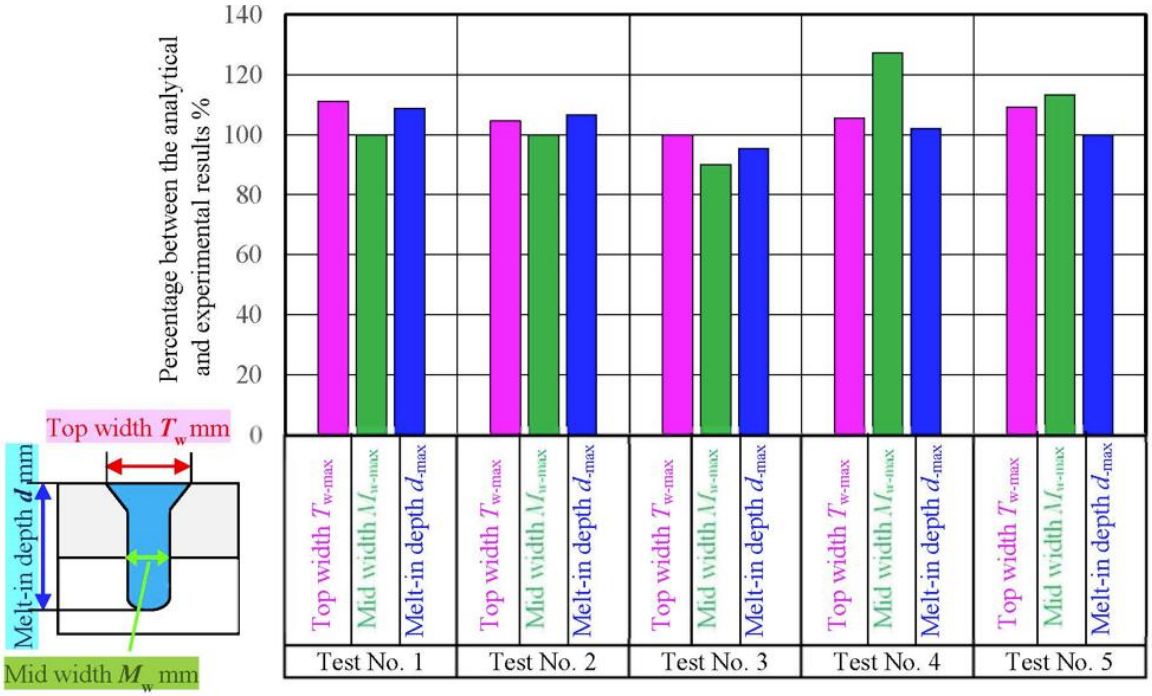

Fig. 20. Percentage of relation between the analytical and experimental results

Percentage of relation between the analytical and experimental results regarding the welding specifications (the maximum top width $T_{w\text{-}max}$, maximum penetration depth d_{max}, and maximum penetration width $M_{w\text{-}max}$) were shown in Figure 20. The percentages between the analytical and experimental results of the maximum top width $T_{w\text{-}max}$ were 100% to 112% (RMSE 9.8%), that of the maximum penetration depth d_{max} were 92% to 126% (RMSE 14.0) and that of the maximum penetration width $M_{w\text{-}max}$ were 94% to 109% (RMSE 6.4%), and the RMSE of total data was 10.6%. Despite using the same simulated thermal conductivities with temperature- dependent in the database, the welding specifications for Test No. 2, No. 3, No.4 and No.5 were calculated with good accuracy, and the proposed FEM simulation technique was considered effective in the search for optimum laser processing conditions.

Furthermore, it should be noted that the proposed technique calculates only the transient temperature distribution during laser keyhole welding using simulated thermal conductivity. Consequently, it is difficult to calculate the mechanical behaviour such as boiling of the molten metal, flow of the molten metal, recrystallisation of the molten metal, and spatter generation. Therefore, whilst the thermal effects of welding speed and laser power on welding specifications can be considered, it is difficult to consider for their mechanical influences on keyhole stability and spatter generation.

5. CONCLUSION

FEM thermal simulation technique for laser keyhole welding was developed and evaluated. The results were summarized as follows;

(1) A new FEM thermal simulation technique using four simulated thermal conductivities has been developed to calculate the melting (fluid) phenomenon and evaporation (gas, keyhole) phenomenon during laser keyhole welding. This enabled the simulation of both melting and evaporation phenomena without the element removal or the remeshing.

(2) The technique could simulate laser irradiation by setting time-dependent heat input conditions.

(3) The percentages between the analytical and experimental results of the maximum top width $T_{w\text{-}max}$ were 100% to 112% (RMSE 9.8%), that of the maximum penetration depth d_{max} were 92% to 126% (RMSE 14.0) and that of the maximum penetration width $M_{w\text{-}max}$ were 94% to 109% (RMSE 6.4%), and the RMSE of total data was 10.6%. The technique was able to analyze welding specifications for overlap keyhole welding of stainless steel SUS304.

REFERENCES

[1] KROLIKOWSKI M., PRZESTACKI D. CHWALCZUK T. SOBOLEWSKA E. TOMASIK M., 2020, *Additive Manufacturing of Polyether Ether Ketone – Peek Parts with Surface Roughness Modification by a Laser Beam*, Journal of Machine Engineering, 20/3, 117–124, ISSN 1895-7595 (Print) ISSN 2391-8071 (Online).

[2] CHWALCZUK T., PRZESTACKI D., SZABLEWSKI P., FELUSIAK A., 2018, *Microstructure Characterization of Inconel 718 After Laser Assisted Turning*, MATEC Web Conf., 188, 02004, https://doi.org/10.1051/matecconf/ 201818802004.

[3] BUDZYN G., RZEPKA J., 2020, *Study on Noises Influencing the Accuracy of CNC Machine Straightness Measurements Methods Based on Beam Position Detection*, Journal of Machine Engineering, 20/3, 76–84, ISSN 1895-7595 (Print) ISSN 2391-8071 (Online).

[4] GUAN G., 2015, *Evaluation of Selective Laser Sintering Processes by Optical Coherence Tomography*, Materials and Design, 88, 837–846.

[5] PEYRE P., 2015, *Experimental and Numerical Analysis of the Selective Laser Sintering (SLS) of PA12 and PEKK Semi-Crystalline Polymers*, Journal of Materials Processing Technology, 225, 326–336.

[6] MILLER R., DEBROY T., 1990, *Energy absorption by Metal-Vapor Dominated Plasma During Carbon Dioxide Laser Welding Of Steels*, Journal of Applied Physics, 68/5, 2045–2050.

[7] SETO N., KATAYAMA S., MATSUNAWA A., 2000, *High-Speed Simultaneous Observation of Plasma and Keyhole Behaviour During High Power CO_2 Laser Welding: Effect of Shielding Gas on Porosity*, Journal of Laser Applications, 12/6, 245–250.

[8] MARTIN R. M., et al., 2018, *High Surface Quality Welding of Aluminium Using Adjustable Ring-Mode Fibre Laser*, Journal of Materials Processing Technology, 258, 180–188.

[9] TANABE I., ISOBE H., 2025, *Development of AI Control Technology for Laser Keyhole Welding*, Proceedings of the 11th World Congress on Electrical Engineering and Computer Systems and Sciences (EECSS'25), https://doi.org/10.11159/CIST25.104., CIST 104-1 to CIST 104-8.

[10] PRZESTACKI D., BARTKOWSKA A., KUKLINSKI M., KIERUJ P., 2018, *The Effects of Laser Surface Modification on the Microstructure of 1.4550 Stainless Steel*, MATEC Web Conf., 237, D2ME, https://doi.org//10.1051/ matecconf/201823702009.

[11] KUKLINSKI M., BARTKOWSKA A., PRZESTACKI D., 2018, *Investigation of Laser Heat Treated Monel 400*, MATEC Web Conf., 219, BalCon, https://doi.org/10.1051/matecconf/201821902005.

[12] CONSORTINI A., RONCHI L., STEFANUTTI L., 1970, *Investigation of Atmospheric Turbulence by Narrow Laser Beams*, Appl. Opt., 9, 2543–2547.

[13] YAHE R.Z., LAST I., 1992, *Numerical Simulation of Laser Beam Propagation in Three-Dimensional Random Media: Beam Splitting and Patch Formation*, Waves in Random Media, 2, 81–98.

[14] ZHAO W., QIU L., FENG Z., LI C., 2006, *Laser Beam Alignment by Fast Feedback Control of Both Linear and Angular Drifts*, Optik, 117, 505.

[15] MURTY S.C.C., 1979, *Laser Beam Propagation in Atmospheric Turbulence*, Prec. Indian Acad. Sci., C 2, Part 2, May, 179–195.

[16] LI Y., QI J., CHEN F., 2017, *Propagation Quality of Laser Diode Beam in Anisotropic Non-Kolmogorov Atmospheric Turbulence*, Acta Optica Sinica, 37/7.
[17] MAHDIEH M.H., 2008, *Numerical Approach to Laser Beam Propagation Through Turbulent Atmosphere and Evaluation of Beam Quality Factor*, Optics Communications, 281, 3395–3402.
[18] NHK, Web feature, Electric vehicles, https://www3.nhk.or.jp/news/html/20221116/k10013893081000.html, (Reference date 23 August 2025.).
[19] SATO Y. S., MIYAKE M., KOKAWA H., OMORI T., ISHIDA K., IMANO S., PARK S.H.C., HIRANO S., 2011, Friction Stir Welding and Processing VI, TMS, 3‑9.
[20] TWI , COREFLOWTM, 2025, *A Sub-Surface Machining Process*, https://www.twi-global.com/media-and-events/insights/coreflow-a-sub-surface-machining-process, (Reference date 23 August 2025).
[21] NGUYEN V.C., LE V.T., PHAM N., NGUYEN A., 2023, *Multi-objective Optimization for Weld Track Geometry in Wire-arc Directed Energy Deposition of ER308L Stainless Steel*, Journal of Machine Engineering, 23/2, 123–134, ISSN 1895-7595 (Print) ISSN 2391-8071 (Online).